JHEP

Published for SISSA by Springer

Received: August 30, 2017
Accepted: September 19, 2017
Published: October 6, 2017

Next-to-leading-order electroweak corrections to the production of three charged leptons plus missing energy at the LHC

Benedikt Biedermann,[a] **Ansgar Denner**[a] **and Lars Hofer**[b]

[a] *Institut für Theoretische Physik und Astrophysik, Julius-Maximilians-Universität Würzburg, Emil-Hilb-Weg 22, 97074 Würzburg, Germany*

[b] *Departament de Física Quàntica i Astrofísica (FQA), Institut de Ciències del Cosmo (ICCUB), Universitat de Barcelona (UB), 08028 Barcelona, Spain*

E-mail: benedikt.biedermann@physik.uni-wuerzburg.de, ansgar.denner@physik.uni-wuerzburg.de, hofer@icc.ub.edu

Abstract: The production of a neutral and a charged vector boson with subsequent decays into three charged leptons and a neutrino is a very important process for precision tests of the Standard Model of elementary particles and in searches for anomalous triple-gauge-boson couplings. In this article, the first computation of next-to-leading-order electroweak corrections to the production of the four-lepton final states $\mu^+\mu^-\mathrm{e}^+\nu_\mathrm{e}$, $\mu^+\mu^-\mathrm{e}^-\bar{\nu}_\mathrm{e}$, $\mu^+\mu^-\mu^+\nu_\mu$, and $\mu^+\mu^-\mu^-\bar{\nu}_\mu$ at the Large Hadron Collider is presented. We use the complete matrix elements at leading and next-to-leading order, including all off-shell effects of intermediate massive vector bosons and virtual photons. The relative electroweak corrections to the fiducial cross sections from quark-induced partonic processes vary between -3% and -6%, depending significantly on the event selection. At the level of differential distributions, we observe large negative corrections of up to -30% in the high-energy tails of distributions originating from electroweak Sudakov logarithms. Photon-induced contributions at next-to-leading order raise the leading-order fiducial cross section by $+2\%$. Interference effects in final states with equal-flavour leptons are at the permille level for the fiducial cross section, but can lead to sizeable effects in off-shell sensitive phase-space regions.

Keywords: NLO Computations

ArXiv ePrint: 1708.06938

https://doi.org/10.1007/JHEP10(2017)043

JHEP10(2017)043

Contents

JHEP10(2017)043

1 Introduction

Vector-boson pair production belongs to the most important process classes at the Large Hadron Collider (LHC). Owing to its sensitivity to the triple-gauge-boson couplings (TGC), it allows for fundamental precision tests of the Standard Model (SM) of elementary particles. In particular, WZ production is considered as one of the key processes in searches for new physics via anomalous TGC. Moreover, WZ production is an important SM background to many direct searches for new physics because the corresponding final state with three charged leptons plus missing energy leads to a relatively clean signature.

Both the ATLAS and CMS collaboration have measured WZ production at 7, 8 and 13 TeV centre-of-mass energy [1–5]. Since the most recent determinations of anomalous TGC from ATLAS data of run II [6] are compatible with the SM prediction, possible new-physics effects are severely constrained and expected to be found by looking for small deviations in high-energy tails of differential distributions. It is thus of prime importance to have precise theoretical predictions for this process at hand.

Most of the efforts for improving the theoretical accuracy of WZ production have been dedicated to perturbative higher-order calculations in the strong coupling α_s. The first next-to-leading order (NLO) QCD computation treating the W and Z boson as on-shell external particles dates back more than two decades [7]. Systematic improvements followed, including leptonic decays [8], off-shell effects and spin correlations [9, 10]. Fixed-order calculations for WZ production have been matched to parton-shower generators at NLO QCD [11–13]. Recently, the first calculation of next-to-next-to-leading order (NNLO) QCD corrections for the integrated cross section has been completed [14] and extended to the level of differential distributions [15].

At this level of accuracy, NLO electroweak (EW) corrections, which are proportional to the electromagnetic coupling α, become relevant as well. On the one hand, naive power

counting $O(\alpha) \approx O(\alpha_s^2)$ suggests that they are of a similar order of magnitude as the NNLO QCD corrections. On the other hand, EW corrections can be enhanced by logarithms of EW origin [16–21] and may distort differential distributions at large transverse momenta by several tens of percent. The latter property is of particular importance, since these phase-space regions are most sensitive to effects of new physics. NLO EW corrections to WZ production have first been studied in a logarithmic approximation [22]. A full NLO EW computation for on-shell W and Z bosons has been presented later on [23, 24] including also photon-induced corrections. The NLO EW corrections for the complete four-lepton-production processes, i.e. including leptonic vector-boson decays and irreducible background diagrams, exist so far only for WW and ZZ production [25–28], while corresponding results for WZ production are still missing in the literature.

The aim of the present article is to fill this gap and to provide results for the NLO EW corrections to the production of three charged leptons plus missing energy at the LHC. We consider the four different and experimentally well-defined final states $\mu^+\mu^-\mathrm{e}^+\nu_\mathrm{e}$, $\mu^+\mu^-\mathrm{e}^-\bar{\nu}_\mathrm{e}$, $\mu^+\mu^-\mu^+\nu_\mu$, and $\mu^+\mu^-\mu^-\bar{\nu}_\mu$. We use the complete matrix elements including besides diagrams with intermediate W and Z bosons also those with virtual photons as well as background diagrams with only one possibly resonant vector boson. In addition, we include also photon-induced contributions at NLO. Using the complex-mass scheme [29–31] for a consistent treatment of resonant propagators, our calculation provides NLO EW predictions for the entire fiducial volume. We apply acceptance cuts inspired by those of the experimental collaborations and study the impact of the corrections on differential observables that are relevant in TGC searches.

This article is organized as follows: in section 2, some details of the computation are outlined. The numerical setup and the phenomenological results are presented in section 3. Finally, conclusions are given in section 4.

2 Details of the calculation

We consider the four independent processes $\mathrm{pp} \to \mu^+\mu^-\mathrm{e}^+\nu_\mathrm{e} + X$, $\mathrm{pp} \to \mu^+\mu^-\mathrm{e}^-\bar{\nu}_\mathrm{e} + X$, $\mathrm{pp} \to \mu^+\mu^-\mu^+\nu_\mu + X$, and $\mathrm{pp} \to \mu^+\mu^-\mu^-\bar{\nu}_\mu + X$. At leading-order (LO), the corresponding hadronic cross sections at $O(\alpha^4)$ in the EW coupling receive contributions from the following partonic channels:

$$\begin{aligned}
&q_i\bar{q}_j/\bar{q}_jq_i \to \mu^+\mu^-\mathrm{e}^+\nu_\mathrm{e}, && q_i\bar{q}_j \in \{\mathrm{u\bar{d}}, \mathrm{c\bar{s}}, \mathrm{u\bar{s}}, \mathrm{c\bar{d}}\},\\
&q_i\bar{q}_j/\bar{q}_jq_i \to \mu^+\mu^-\mu^+\nu_\mu, && q_i\bar{q}_j \in \{\mathrm{u\bar{d}}, \mathrm{c\bar{s}}, \mathrm{u\bar{s}}, \mathrm{c\bar{d}}\},\\
&q_i\bar{q}_j/\bar{q}_jq_i \to \mu^+\mu^-\mathrm{e}^-\bar{\nu}_\mathrm{e}, && q_i\bar{q}_j \in \{\mathrm{d\bar{u}}, \mathrm{s\bar{c}}, \mathrm{s\bar{u}}, \mathrm{d\bar{c}}\},\\
&q_i\bar{q}_j/\bar{q}_jq_i \to \mu^+\mu^-\mu^-\bar{\nu}_\mu, && q_i\bar{q}_j \in \{\mathrm{d\bar{u}}, \mathrm{s\bar{c}}, \mathrm{s\bar{u}}, \mathrm{d\bar{c}}\}.
\end{aligned} \tag{2.1}$$

We include quark-flavour mixing between the first two quark families as described by the Cabibbo-Kobayashi-Maskawa (CKM) matrix defined in eq. (3.5), i.e. we take into account first-order mixing but neglect any higher-order quark-flavour mixings. The dominant channels involving only quarks and antiquarks of the first generation contribute about 80% to the integrated LO cross section, the corresponding channels of the second family between

JHEP10(2017)043

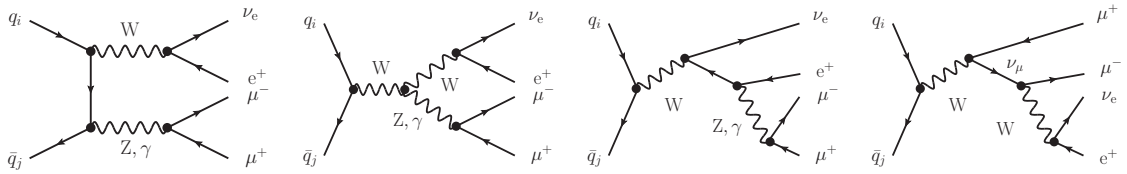

Figure 1. Sample tree-level diagrams contributing at $O(\alpha^4)$ to $q_i\bar{q}_j \to \mu^+\mu^-e^+\nu_e$.

10% and 20%. Channels involving quarks of the first and anti-quarks of the second generation or vice versa, stay at the percent level. Sample tree-level diagrams contributing to the process $q_i\bar{q}_j \to \mu^+\mu^-e^+\nu_e$ are shown in figure 1. Besides diagrams with a resonant W boson and a resonant Z boson or a photon these involve also diagrams with only one possibly resonant vector boson.

The NLO EW corrections at $O(\alpha^5)$ comprise virtual corrections to the partonic channels (2.1) as well as real photon emission via the quark-induced channels

$$\begin{aligned}
&q_i\bar{q}_j/\bar{q}_jq_i \to \mu^+\mu^-e^+\nu_e\,(+\gamma), && q_i\bar{q}_j \in \{u\bar{d}, c\bar{s}, u\bar{s}, c\bar{d}\},\\
&q_i\bar{q}_j/\bar{q}_jq_i \to \mu^+\mu^-\mu^+\nu_\mu\,(+\gamma), && q_i\bar{q}_j \in \{u\bar{d}, c\bar{s}, u\bar{s}, c\bar{d}\},\\
&q_i\bar{q}_j/\bar{q}_jq_i \to \mu^+\mu^-e^-\bar{\nu}_e\,(+\gamma), && q_i\bar{q}_j \in \{d\bar{u}, s\bar{c}, s\bar{u}, d\bar{c}\},\\
&q_i\bar{q}_j/\bar{q}_jq_i \to \mu^+\mu^-\mu^-\bar{\nu}_\mu\,(+\gamma), && q_i\bar{q}_j \in \{d\bar{u}, s\bar{c}, s\bar{u}, d\bar{c}\}.
\end{aligned} \tag{2.2}$$

Moreover, we include the photon-induced contributions with one (anti)quark and one photon in the initial state,

$$\begin{aligned}
&\gamma q_i/q_i\gamma \to \mu^+\mu^-e^+\nu_e\,q_j, && q_iq_j \in \{ud, cs\},\\
&\gamma \bar{q}_i/\bar{q}_i\gamma \to \mu^+\mu^-e^+\nu_e\,\bar{q}_j, && \bar{q}_i\bar{q}_j \in \{\bar{d}\bar{u}, \bar{s}\bar{c}\},\\
&\gamma q_i/q_i\gamma \to \mu^+\mu^-\mu^+\nu_\mu\,q_j, && q_iq_j \in \{ud, cs\},\\
&\gamma \bar{q}_i/\bar{q}_i\gamma \to \mu^+\mu^-\mu^+\nu_\mu\,\bar{q}_j, && \bar{q}_i\bar{q}_j \in \{\bar{d}\bar{u}, \bar{s}\bar{c}\},\\
&\gamma q_i/q_i\gamma \to \mu^+\mu^-e^-\bar{\nu}_e\,q_j, && q_iq_j \in \{du, sc\},\\
&\gamma \bar{q}_i/\bar{q}_i\gamma \to \mu^+\mu^-e^-\bar{\nu}_e\,\bar{q}_j, && \bar{q}_i\bar{q}_j \in \{\bar{u}\bar{d}, \bar{c}\bar{s}\},\\
&\gamma q_i/q_i\gamma \to \mu^+\mu^-\mu^-\bar{\nu}_\mu\,q_j, && q_iq_j \in \{du, sc\},\\
&\gamma \bar{q}_i/\bar{q}_i\gamma \to \mu^+\mu^-\mu^-\bar{\nu}_\mu\,\bar{q}_j, && \bar{q}_i\bar{q}_j \in \{\bar{u}\bar{d}, \bar{c}\bar{s}\},
\end{aligned} \tag{2.3}$$

generically referred to as $q\gamma$ channels in the following. In all considered contributions, the bottom quark can neither appear as initial-state nor final-state particle since its weak isospin partner, the top quark, is by construction excluded as external particle in all considered partonic channels at LO and NLO.

Since all considered processes involve exactly one quark-flavour-changing vertex at tree level and since we treat all quarks except the top quark as massless, all tree-level amplitudes can be constructed by multiplying the amplitudes for a unit CKM matrix with the corresponding non-vanishing CKM matrix elements. This treatment is also exact for

JHEP10(2017)043

the real and virtual corrections in our setup. Since the CKM matrix can be eliminated for massless down-type quarks by a redefinition of flavour eigenstates, no renormalization of the CKM matrix is required in this approximation. Non-trivial CKM effects only enter because the flavour symmetry is broken when amplitudes for different quark flavours are weighted with different parton distribution functions (PDFs). For the photon-induced channels the CKM matrix drops out exactly owing to its unitarity when the sum over the flavour of the final-state quark is performed. For that reason, we can restrict the evaluation of the corrections in (2.3) to flavour-diagonal channels with the CKM matrix set to unity.

The one-loop virtual corrections comprise the full set of Feynman diagrams to the processes (2.1) at order $O(\alpha^5)$. Both at tree and one-loop level, we employ the complex-mass scheme for a consistent treatment of massive resonant particles [29–31] leading to NLO EW accuracy everywhere in phase space. The integration of the real corrections is performed with help of the subtraction methods of refs. [32, 33] in order to deal with soft and collinear photon emission off fermions and with the collinear initial-state singularities in the photon-induced corrections. The employed formalism extends the dipole subtraction from QCD [34] to the case with QED splittings. The general idea of subtraction methods is to add and subtract auxiliary terms that mimic the singularity structure of the real squared matrix elements point-wise such that the resulting differences can be integrated in four space-time dimensions. The re-added subtraction terms, on the other hand, can be integrated in a process-independent way allowing for an isolation of the divergences of the real corrections in analytical form. For infrared-safe observables, the extracted collinear final-state singularities and the soft singularities cancel with the corresponding divergences from the one-loop corrections according to the Kinoshita-Lee-Nauenberg theorem. The left-over collinear initial-state singularities are absorbed in redefined parton-distribution functions. A more detailed description of real and virtual NLO EW corrections to vector-boson pair production is given in ref. [26] for the more general case of the production of four charged leptons.

The full computation with all possible final states has been performed with a private Monte Carlo program that has already successfully been used for the integration of the NLO EW corrections to ZZ and WW production [25–27] and for the NLO QCD and EW corrections to vector-boson scattering [35, 36]. All the tree-level and one-loop matrix elements for LO, real and virtual contributions have been evaluated with the computer program Recola [37] which internally uses the Collier library [38] for the one-loop scalar [39–42] and tensor integrals [43–45]. As a cross check, we have performed an independent calculation of the process $pp \to \mu^+\mu^-e^+\nu_e + X$ and found perfect agreement at the level of phase-space points and at the level of differential cross sections within the statistical uncertainty of the Monte Carlo integration. The matrix elements of the second implementation are generated with the Mathematica package Pole [46] which is based on FeynArts [47, 48] and FormCalc [49]. The phase-space integration is carried out with an independent multi-channel Monte Carlo integrator based on the ones described in refs. [50, 51].

JHEP10(2017)043

3 Phenomenological results

3.1 Input parameters

For the numerical analysis we choose the following input parameters based on ref. [52]. The on-shell masses and widths of the gauge bosons read

$$\begin{aligned} M_{\mathrm{Z}}^{\mathrm{os}} &= 91.1876\,\mathrm{GeV}, & \Gamma_{\mathrm{Z}}^{\mathrm{os}} &= 2.4952\,\mathrm{GeV}, \\ M_{\mathrm{W}}^{\mathrm{os}} &= 80.385\,\mathrm{GeV}, & \Gamma_{\mathrm{W}}^{\mathrm{os}} &= 2.085\,\mathrm{GeV}. \end{aligned} \tag{3.1}$$

For the use within the complex-mass scheme, they need to be converted to pole masses and widths according to ref. [53]:

$$M = \frac{M^{\mathrm{os}}}{\sqrt{1+(\Gamma^{\mathrm{os}}/M^{\mathrm{os}})^2}}, \qquad \Gamma = \frac{\Gamma^{\mathrm{os}}}{\sqrt{1+(\Gamma^{\mathrm{os}}/M^{\mathrm{os}})^2}}. \tag{3.2}$$

For the masses of the Higgs boson and the top quark, we use

$$M_{\mathrm{H}} = 125\,\mathrm{GeV}, \qquad m_{\mathrm{t}} = 173\,\mathrm{GeV}, \tag{3.3}$$

while their widths can be set equal to zero as they do not appear as internal resonances in the considered processes. Throughout the calculation, all the charged leptons $\ell = \{\mathrm{e}^{\pm}, \mu^{\pm}, \tau^{\pm}\}$ and the five quarks $q = \{\mathrm{u}, \mathrm{d}, \mathrm{c}, \mathrm{s}, \mathrm{b}\}$ are considered as light particles with negligible masses.

The electromagnetic coupling α is derived from the Fermi constant according to

$$\alpha_{G_\mu} = \frac{\sqrt{2}}{\pi} G_\mu M_{\mathrm{W}}^2 \left(1 - \frac{M_{\mathrm{W}}^2}{M_{\mathrm{Z}}^2}\right) \qquad \text{with} \qquad G_\mu = 1.16637 \times 10^{-5}\,\mathrm{GeV}^{-2}, \tag{3.4}$$

i.e. we work in the G_μ scheme. In this scheme, the effects of the running of α from zero-momentum transfer to the electroweak scale are absorbed into the LO cross section, and mass singularities in the charge renormalization are avoided. Moreover, α_{G_μ} partially accounts for the leading universal renormalization effects related to the ρ-parameter. We use the following approximation for the CKM matrix that includes transitions between the first two quark generations:

$$V_{\mathrm{CKM}} = \begin{pmatrix} V_{\mathrm{ud}} & V_{\mathrm{us}} & V_{\mathrm{ub}} \\ V_{\mathrm{cd}} & V_{\mathrm{cs}} & V_{\mathrm{cb}} \\ V_{\mathrm{td}} & V_{\mathrm{ts}} & V_{\mathrm{tb}} \end{pmatrix} = \begin{pmatrix} \cos\theta_{\mathrm{c}} & \sin\theta_{\mathrm{c}} & 0 \\ -\sin\theta_{\mathrm{c}} & \cos\theta_{\mathrm{c}} & 0 \\ 0 & 0 & 1 \end{pmatrix}, \qquad \sin\theta_{\mathrm{c}} = 0.225. \tag{3.5}$$

Following ref. [15], the renormalisation and factorisation scales, μ_{ren} and μ_{fact}, are set equal to the average of the Z-boson and W-boson mass,

$$\mu_{\mathrm{ren}} = \mu_{\mathrm{fact}} = (M_{\mathrm{Z}} + M_{\mathrm{W}})/2. \tag{3.6}$$

As PDFs we choose the `LUXqed_plus_PDF4LHC15_nnlo_100` parameterisation [54, 55]. Throughout our calculation, we employ the $\overline{\mathrm{MS}}$ factorisation scheme. We have numerically verified that the difference between this scheme and the often used deep-inelastic-scattering scheme is below one permille for the relative NLO EW corrections and, thus, phenomenologically irrelevant.

JHEP10(2017)043

3.2 Observable definition and acceptance cuts

Photons emitted in the Bremsstrahlung corrections are recombined with the closest charged lepton if their separation ΔR in the rapidity-azimuthal-angle plane fulfils

$$\Delta R_{\ell_i,\gamma} = \sqrt{(y_{\ell_i} - y_\gamma)^2 + (\Delta\phi_{\ell_i,\gamma})^2} < 0.1, \tag{3.7}$$

where y denotes the rapidity of the final-state particle and $\Delta\phi_{\ell_i,\gamma}$ the azimuthal-angle difference between a charged lepton ℓ_i and the photon γ. Final-state photons with rapidity $|y_\gamma| > 5$ are considered as lost in the beam pipe and excluded from recombination. Final-state jets present in the photon-induced real corrections are not recombined with any other particle.

We refer to $(\ell_{\mathrm{Z}}^+\ell_{\mathrm{Z}}^-)$ as the lepton pair associated with the Z-boson decay and to $\ell_{\mathrm{W}}^\pm$ as the charged lepton from the W-boson decay. For the processes involving both muons and electrons, the equal-flavour lepton pair is associated with the Z-boson decay, while the other charged lepton is associated with the W-boson decay. For the processes with three equal-flavour leptons in the final state, the lepton pair emerging from the Z-boson decay is defined as the one whose invariant mass $M_{\ell_i^+,\ell_j^-}$ is closer to the nominal Z-boson mass.

We have investigated each process class in two different scenarios: first with a minimal set of selection cuts, in the following referred to as "inclusive setup", and second for a setup inspired by the ATLAS measurements [2, 3] that is tailored to the investigation of TGC, referred to as "TGC setup". The corresponding fiducial volumes are defined as follows:

Inclusive setup. We treat all charged final-state leptons on the same footing, requiring

$$p_{\mathrm{T},\ell_i} > 15\,\mathrm{GeV}, \qquad |y_{\ell_i}| < 2.5, \qquad \Delta R_{\ell_i,\ell_j} > 0.2, \tag{3.8}$$

where p_{T} denotes the transverse momentum.

Exclusive setup for TGC analysis. For each charged lepton ℓ_i, we demand a minimal transverse momentum and a maximal rapidity:

$$p_{\mathrm{T},\ell_{\mathrm{Z}}} > 15\,\mathrm{GeV}, \qquad p_{\mathrm{T},\ell_{\mathrm{W}}} > 20\,\mathrm{GeV}, \qquad |y_{\ell_i}| < 2.5. \tag{3.9}$$

Any pair of charged leptons (ℓ_i, ℓ_j) is required to be well separated in the rapidity-azimuthal-angle plane:

$$\Delta R_{\ell_{\mathrm{Z}},\ell_{\mathrm{Z}}} > 0.2, \qquad \Delta R_{\ell_{\mathrm{Z}},\ell_{\mathrm{W}}} > 0.3. \tag{3.10}$$

The invariant mass of the $\ell_{\mathrm{Z}}^+\ell_{\mathrm{Z}}^-$ pair is allowed to differ by at most 10 GeV from the nominal Z-boson mass:

$$M_{\mathrm{Z}} - 10\,\mathrm{GeV} < M_{\ell_{\mathrm{Z}}^+,\ell_{\mathrm{Z}}^-} < M_{\mathrm{Z}} + 10\,\mathrm{GeV}. \tag{3.11}$$

The W-boson transverse mass $M_{\mathrm{T}}^{\mathrm{W}}$ must obey

$$M_{\mathrm{T}}^{\mathrm{W}} = \sqrt{2p_{\mathrm{T}}^{\mathrm{miss}} p_{\mathrm{T},\ell_{\mathrm{W}}}[1 - \cos\Delta\phi(\ell_{\mathrm{W}}, \vec{p}_{\mathrm{T}}^{\,\mathrm{miss}})]} > 30\,\mathrm{GeV}, \tag{3.12}$$

JHEP10(2017)043

mixed flavour $[2\mu e\nu]$		σ_{LO} [fb]	$\delta_{\bar{q}q'}(\%)$	$\delta_{q\gamma}(\%)$	$\delta_{\mathrm{NLO}}(\%)$
inclusive	$pp \to \mu^+\mu^-e^+\nu_e + X$	27.303(1)	−3.308(5)	+1.9564(4)	−1.351(5)
inclusive	$pp \to \mu^+\mu^-e^-\bar{\nu}_e + X$	17.9133(7)	−3.211(5)	+2.1004(4)	−1.111(5)
TGC	$pp \to \mu^+\mu^-e^+\nu_e + X$	19.1625(6)	−5.986(6)	+1.6971(3)	−4.289(6)
TGC	$pp \to \mu^+\mu^-e^-\bar{\nu}_e + X$	12.8624(4)	−5.950(6)	+1.7908(3)	−4.160(6)
equal flavour $[3\mu\nu]$		σ_{LO} [fb]	$\delta_{\bar{q}q'}(\%)$	$\delta_{q\gamma}(\%)$	$\delta_{\mathrm{NLO}}(\%)$
inclusive	$pp \to \mu^+\mu^-\mu^+\nu_\mu + X$	27.2448(9)	−3.310(4)	+1.9577(4)	−1.352(4)
inclusive	$pp \to \mu^+\mu^-\mu^-\bar{\nu}_\mu + X$	17.8621(6)	−3.203(4)	+2.1030(4)	−1.100(4)
TGC	$pp \to \mu^+\mu^-\mu^+\nu_\mu + X$	19.4353(6)	−5.709(5)	+1.7155(4)	−3.993(5)
TGC	$pp \to \mu^+\mu^-\mu^-\bar{\nu}_\mu + X$	13.0398(4)	−5.661(5)	+1.8101(3)	−3.851(5)

Table 1. Fiducial cross sections with first-order quark-flavour mixings for all considered final states in the inclusive and TGC setup.

where $\Delta\phi(\ell_{\mathrm{W}}, \vec{p}_{\mathrm{T}}^{\,\mathrm{miss}})$ denotes the azimuthal angle between the momentum of the W-boson decay lepton ℓ_{W} and the missing momentum in the transverse plane $\vec{p}_{\mathrm{T}}^{\,\mathrm{miss}}$, and $p_{\mathrm{T}}^{\mathrm{miss}} = |\vec{p}_{\mathrm{T}}^{\,\mathrm{miss}}|$.

We define the missing momentum as the negative vector sum of the momenta of all observed particles. Final-state quarks from the photon-induced corrections are considered as observable jets if their transverse momentum satisfies

$$p_{\mathrm{T}}^{\mathrm{jet}} > p_{\mathrm{T,min}}^{\mathrm{jet}} = 25\,\mathrm{GeV}. \tag{3.13}$$

Hence, quarks in the final state with transverse momentum below $p_{\mathrm{T,min}}^{\mathrm{jet}}$ contribute to the missing momentum. All photons and jets from real radiation with rapidity $|y_{\gamma/\mathrm{jet}}| > 5$ are considered as lost in the beam pipe, and their four-momentum, thus, contributes to the missing momentum as well. We note that with this definition, the missing momentum coincides with the neutrino momentum at LO but not necessarily at NLO.

3.3 Results on integrated cross sections

The results for the fiducial cross sections at a centre-of-mass energy of 13 TeV are presented in table 1 for all considered final states both in the inclusive and in the TGC setup. The second column shows the absolute prediction for the cross section at leading order, σ_{LO}, followed by the relative EW corrections of the quark-induced contributions $\delta_{\bar{q}q'}$, the relative photon-induced corrections $\delta_{q\gamma}$, and the total relative EW corrections $\delta_{\mathrm{NLO}} = \delta_{\bar{q}q'} + \delta_{q\gamma}$. According to the total electric charge of the final-state leptons, we sometimes refer to the processes $pp \to \mu^+\mu^-e^+\nu_e + X$ and $pp \to \mu^+\mu^-\mu^+\nu_\mu + X$ as ZW^+ and to the processes $pp \to \mu^+\mu^-e^-\bar{\nu}_e + X$ and $pp \to \mu^+\mu^-\mu^-\bar{\nu}_\mu + X$ as ZW^-. We stress, however, that we include all contributions leading to the considered four-lepton final state, also those which do not proceed through intermediate $ZW^\pm$ production. The cross sections for the ZW^+ channels are about 50% larger than the ones for the ZW^- channels, both in the mixed-flavour case $[2\mu e\nu]$ and in the equal-flavour case $[3\mu\nu]$. This can be attributed to the

JHEP10(2017)043

parton flux within the proton which is larger for the up quark than for the down quark. The fiducial cross section in the TGC setup is about 30% smaller than in the inclusive setup, as expected owing to the reduced fiducial volume. For all setups and channels, the photon-induced contributions are of the order of +2% with only minor variations at the subpercent level. The quark-induced EW corrections are negative and depend significantly on the phase-space cuts. The corrections in the TGC setup are with about −6% almost twice as large as in the inclusive setup where they reach about −3%. The main reason for the large difference is the invariant-mass cut in eq. (3.11) which partially removes the radiative tail below the Z-boson invariant mass as illustrated in the next section in the context of differential distributions (cf. figure 2). Switching off the invariant-mass cut in the TGC setup leads to EW corrections in the quark-induced channels of $\sim -3.5\%$, i.e. much closer to the results from the inclusive setup. Owing to the opposite sign of the photon-induced and quark-induced corrections, the net corrections to the fiducial cross section are only about −1% in the inclusive setup and remain around −4% in the TGC setup.

The inclusion of first-order transitions in flavour-changing currents lowers the total cross section with respect to a unit CKM matrix by 0.7% in the ZW^+ channels and by 0.9% in the ZW^- channels independently of the leptons in the final state. We have also performed a LO study including transitions between the second and third quark generation, which prooved that this effect is phenomenologically irrelevant.

Since the cuts of the inclusive setup are by construction not sensitive to the lepton pairing, the scenario is well suited to study the size of interference effects present for equal-flavour leptons in the final state. In the absence of any interference, the equal-flavour and mixed-flavour cross sections would be equal. The deviation of the ratio $\sigma^{[3\mu\nu]}/\sigma^{[2\mu e\nu]}$ from one thus gives a measure of the impact of interferences. At LO, we find $\sigma^{\mu^+\mu^-\mu^+\nu_\mu}/\sigma^{\mu^+\mu^-\mathrm{e}^+\nu_\mathrm{e}} = 0.99785(5)$ and $\sigma^{\mu^+\mu^-\mu^-\bar{\nu}_\mu}/\sigma^{\mu^+\mu^-\mathrm{e}^-\bar{\nu}_\mathrm{e}} = 0.99714(5)$. Hence, the interferences lower the LO cross sections at the permille level. The interference effect on the relative NLO EW corrections is far below the permille level and phenomenologically unimportant for the fiducial cross section. We conclude that, in an inclusive scenario, the theory prediction for the integrated NLO EW cross section can be covered both for the mixed-flavour and equal-flavour final state by a single computation. In the TGC scenario, the interference effects cannot be isolated uniquely as the phase-space cuts are not symmetric under the exchange of the two identical final-state leptons. It is thus not surprising to find larger deviations of 1.4% from the unit ratio [$\sigma^{\mu^+\mu^-\mu^+\nu_\mu}/\sigma^{\mu^+\mu^-\mathrm{e}^+\nu_\mathrm{e}} = 1.01424(5)$ and $\sigma^{\mu^+\mu^-\mu^-\bar{\nu}_\mu}/\sigma^{\mu^+\mu^-\mathrm{e}^-\bar{\nu}_\mathrm{e}} = 1.01379(5)$].

We conclude this section with a comparison of our results for the fiducial cross section with those in the literature for on-shell WZ production. The computation of ref. [24] includes photon-induced and quark-induced corrections, and states for the total cross section (no phase-space cuts applied) a negligible EW correction. Unfortunately, there are no separate numbers for the $q\gamma$ and $\bar{q}q'$ channels for a detailed comparison. The computation in ref. [23] does not include photon-induced corrections. For the LHC at 14 TeV, the authors state corrections of $\delta_{\bar{q}q'} = -1.5\%$ for ZW^+ and $\delta_{\bar{q}q'} = -1.3\%$ for ZW^-, applying a minimal event selection that is roughly comparable with our inclusive setup. We attribute the difference of 2% to our results mainly to photon radiation off the $\mu^+\mu^-$ pair. Inspection

JHEP10(2017)043

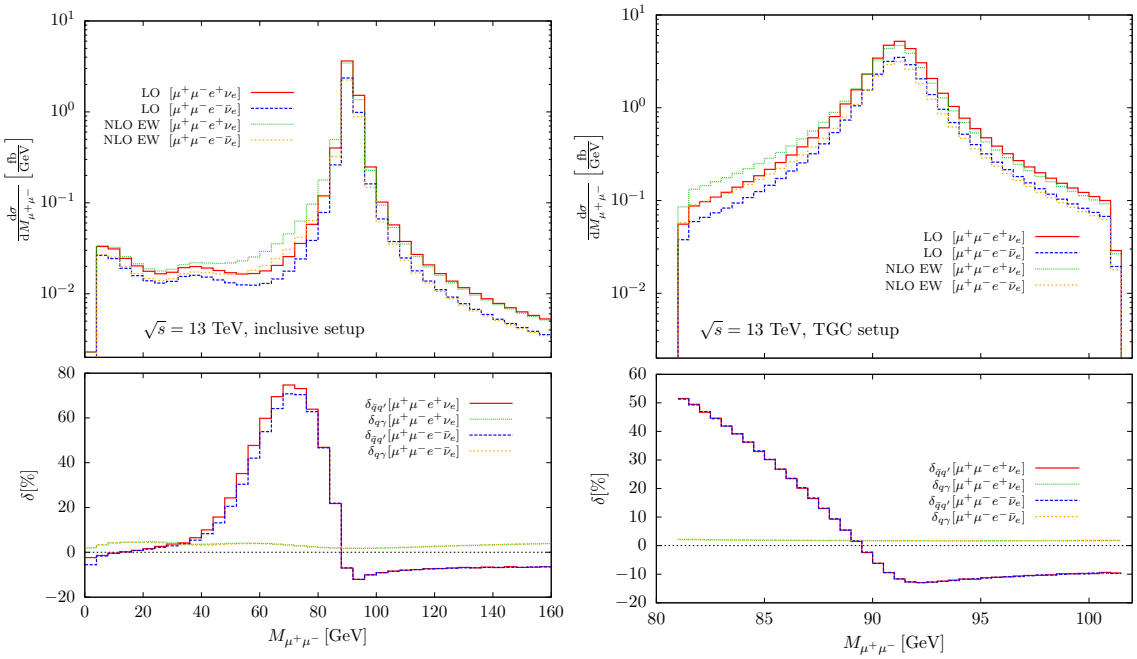

Figure 2. Distribution in the invariant mass of the $\mu^+\mu^-$ pair in the inclusive setup (left panel) and in the TGC setup (right panel).

of the (unmeasurable) four-lepton invariant-mass distribution reveals that above the pair-production threshold, where the cross section receives the largest contribution, the NLO EW corrections are negative at the level of -3% and dominated by real photon radiation. For an on-shell Z boson, the effect of final-state radiation and thus of real corrections is reduced.

3.4 Results on differential cross sections

In the following, we present results for distributions for the LHC at 13 TeV. In each of the figures, the upper panels show the absolute predictions for the LO and NLO differential cross section while the lower panels display the relative EW corrections.

We first discuss the mixed-flavour final state where the $\mu^+\mu^-$ pair can be associated with the decay of the neutral vector boson, distinguishing between the ZW^+ and ZW^- case. Figure 2 shows the invariant-mass distributions of the $\mu^+\mu^-$ system. The absolute prediction in the inclusive setup (left panel) exhibits the characteristic pattern of this observable similar to the corresponding $\mu^+\mu^-$ invariant-mass distribution in ZZ production in ref. [26]: 1) the resonance peak at $M_{\mu^+\mu^-} = M_Z$, 2) the increase of the cross section towards $M_{\mu^+\mu^-} = 0$ owing to the tail of the photon pole, and 3) a little bump between 30 GeV and 50 GeV from the s-channel resonance at $M_{\mu^+\mu^-e^\pm(\bar{\nu})_e} = M_W$ [cf. diagrams (b), (c) and (d) in figure 1]. Turning to the EW corrections, we observe in the quark-induced channels a typical radiative tail with corrections of up to +75%: photon radiation off the final-state charged leptons may shift the measured value of the invariant mass to lower values. Since the LO cross section falls off steeply below the resonance, the relative real NLO corrections become large. At the resonance the corrections change sign, and above

JHEP10(2017)043

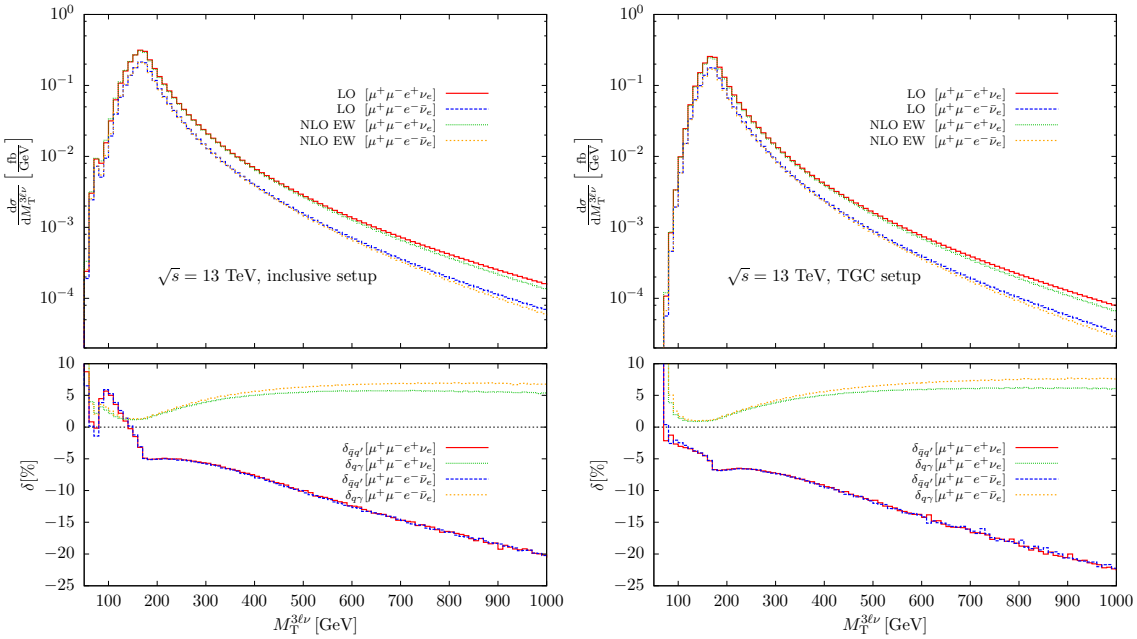

Figure 3. Distribution in the transverse mass of the four-lepton system in the inclusive setup (left panel) and in the TGC setup (right panel).

they are of the order of -10% (they reach -25% at 1.5 TeV, not shown in the plot). The relative EW corrections are almost equal for ZW^+ and ZW^-, the only visible difference being in the radiative tail which is up to 6% larger for ZW^+. This difference results from folding the partonic cross sections with the PDFs. The photon-induced corrections are positive over the whole spectrum with variations between 1.8% and 5%. Owing to the cut around the Z-boson resonance (3.11), the invariant $\mu^+\mu^-$ mass in the TGC scenario (right panel) is restricted to $[M_Z - 10, M_Z + 10]$. Evidently, this cut removes a substantial part of the radiative tail present in the inclusive setup.

Figure 3 shows the distribution in the transverse mass $M_T^{3\ell\nu}$ of the four-lepton system in the inclusive setup (left panel) and in the TGC setup (right panel) as defined in ref. [2],

$$M_T^{3\ell\nu} = \sqrt{\left(\sum_{\ell_i=1}^{3} p_{T,\ell_i} + |\vec{p}_T^{\,\text{miss}}|\right)^2 - \left[\left(\sum_{\ell_i=1}^{3} p_{\ell_i,x} + p_x^{\text{miss}}\right)^2 + \left(\sum_{\ell_i=1}^{3} p_{\ell_i,y} + p_y^{\text{miss}}\right)^2\right]} \tag{3.14}$$

with $\ell_1 = \ell_Z^+$, $\ell_2 = \ell_Z^-$, $\ell_3 = \ell_W^\pm$ and the missing momentum $\vec{p}^{\,\text{miss}}$ defined at the end of section 3.2. Note that for contributions with only leptons in the final state, like the virtual corrections or the LO contribution, the transverse mass in eq. (3.14) reduces to the scalar sum of the lepton transverse momenta. The absolute prediction has its maximum slightly below $M_T^{3\ell\nu} = M_Z + M_W$. The observable does not show a sharp pair-production threshold (like the unmeasurable four-lepton invariant-mass distribution would exhibit at $M_{4\ell} = M_Z + M_W$, cf. the discussion in ref. [26] for ZZ production) as the unmeasurable boost of the four-lepton system along the beam axis allows for on-shell production of the

JHEP10(2017)043

W and Z boson below $M_{\mathrm{T}}^{3\ell\nu} = M_{\mathrm{Z}} + M_{\mathrm{W}}$. The little peak directly below 80 GeV in the inclusive setup stems from a single W-boson resonance with $M_{\mathrm{W}}^2 = (p_{\ell_{\mathrm{Z}}^+} + p_{\ell_{\mathrm{Z}}^-} + p_{\ell_{\mathrm{W}}^\pm} + p_\nu)^2$ [cf. diagrams (b), (c) and (d) in figure 1]. This resonance is removed in the TGC setup owing to the lower cut on the invariant $\mu^+\mu^-$ mass in eq. (3.11) and the minimal transverse momentum $p_{\mathrm{T},\ell_{\mathrm{W}}}^{\mathrm{min}}$ of the charged W-decay lepton candidate in eq. (3.9) since $(M_{\mathrm{Z}} - 10\,\mathrm{GeV}) + p_{\mathrm{T},\ell_{\mathrm{W}}}^{\mathrm{min}} > M_{\mathrm{W}}$. The shape of the quark-induced EW corrections above the maximum of the distribution is very similar in both setups. We observe a plateau region from the maximum on up to about 300 GeV with -5% corrections in the inclusive setup (-7% in the TGC setup) and then a constant decrease to -20% (-22%) at 1 TeV. The shape of the NLO EW corrections can be understood best by analysing the contributions from the subtracted virtual and real corrections separately. Up to about 250 GeV, the subtracted virtual corrections contribute less than one percent, above 250 GeV, however, they grow negative with constant slope and dominate the entire high-energy behaviour owing to EW Sudakov logarithms. Above the maximum of the distribution, the subtracted real corrections cause a flat off-set and only slightly decrease in magnitude with growing $M_{\mathrm{T}}^{3\ell\nu}$. The combination of the virtual and real corrections gives rise to the plateau in the distribution. The region below the maximum is entirely dominated by the subtracted real corrections: the kink at the maximum followed by increasing corrections is due to the radiative return of the real photon at the relatively broad peak. The difference between the TGC and the inclusive setup in this region results from the enhanced radiative tail from the reconstructed Z-boson resonance, as we checked explicitly by switching off the invariant-mass cut in eq. (3.11). The photon-induced corrections have their minimum with about 1% where the LO quark-induced channels are largest, and constantly increase with growing $M_{\mathrm{T}}^{3\ell\nu}$ up to 5% to 8%, depending on the final state and the setup.

Figure 4 compares the transverse mass $M_{\mathrm{T}}^{3\ell\nu}$ of the four-lepton system for the equal-flavour $[3\mu\nu]$ and mixed-flavour $[2\mu\mathrm{e}\nu]$ final states in ZW^+ production for the inclusive setup (left panel) and for the TGC setup (right panel). For both scenarios, the relative EW corrections of the $\mu^+\mu^-\mathrm{e}^+\nu_{\mathrm{e}}$ and $\mu^+\mu^-\mu^+\nu_\mu$ final states are almost equal (separately for the $\bar{q}q'$ and $q\gamma$ channels). This is in agreement with the results for the fiducial cross section where only permille-level differences between corrections of the mixed- and equal-flavour final states are observed. In the lowest panel, the ratio $(\mathrm{d}\sigma_{(\mathrm{N})\mathrm{LO}}^{[3\mu\nu]}/\mathrm{d}M_{\mathrm{T}}^{3\ell\nu})/(\mathrm{d}\sigma_{(\mathrm{N})\mathrm{LO}}^{[2\mu\mathrm{e}\nu]}/\mathrm{d}M_{\mathrm{T}}^{3\ell\nu})$ is shown. By construction, the observable $M_{\mathrm{T}}^{3\ell\nu}$ is not sensitive to the assignment of the decay leptons to the Z or the W boson. Since the inclusive setup is symmetric in the equal-flavour final-state leptons, the deviation from one of this ratio gives a direct measure of the impact of interferences. In the off-shell-sensitive region below 100 GeV, the interferences become indeed sizeable, lowering the $[3\mu\nu]$ cross section by about one third with respect to the $[2\mu\mathrm{e}\nu]$ case. As expected, the interferences are irrelevant in the on-shell region, where they are suppressed with respect to the doubly-resonant contributions. In the TGC setup we observe relative differences between the two final states of the order of 2–3% also in the on-shell region. Because of the smallness of the interference effects in the inclusive setup we attribute the deviation from one in the on-shell region in the TGC setup to the lepton pairing in the presence of asymmetric cuts on ℓ_{W} and ℓ_{Z}. Around the maximum, the ratio deviates from one at the percent level, in agreement with the ratio for the fiducial

JHEP10(2017)043

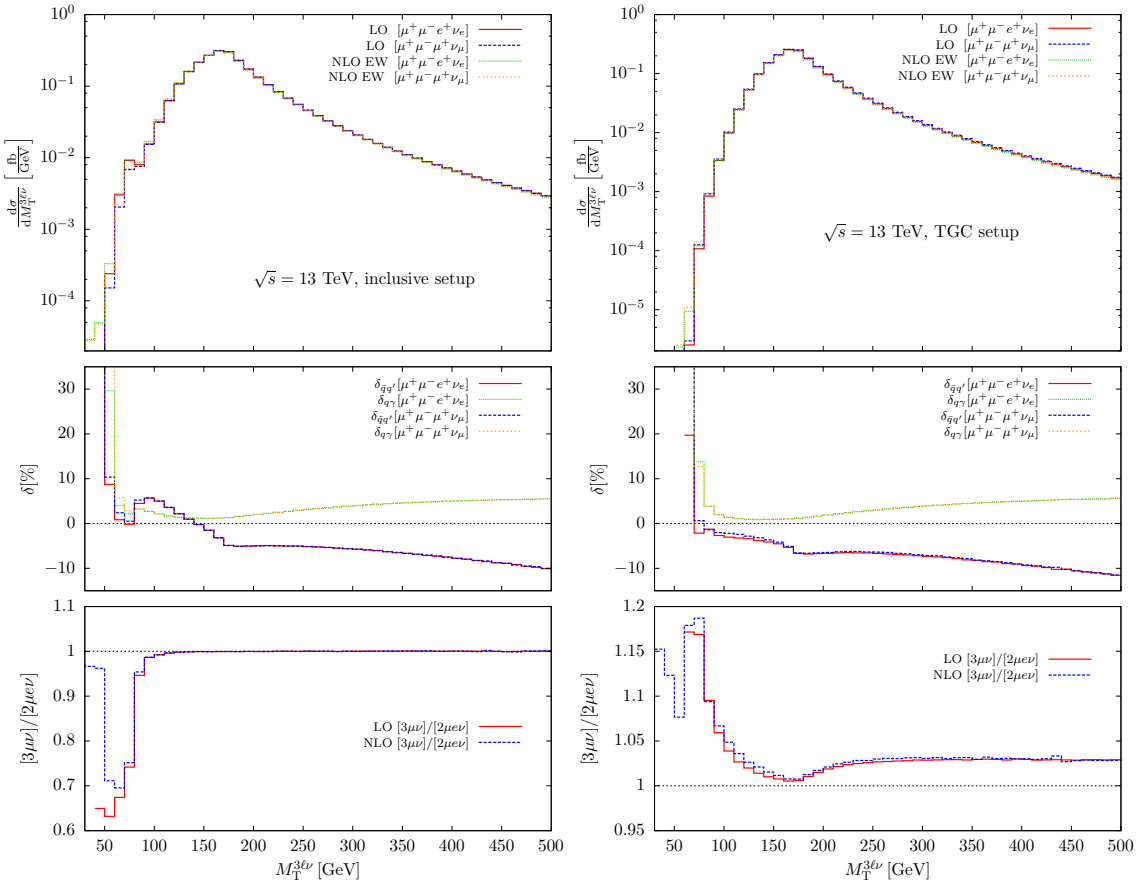

Figure 4. Comparison between equal-flavour and mixed-flavour final state for the distribution in the four-lepton transverse mass $M_T^{3\ell\nu}$ for ZW^+ production. The left panel shows the inclusive setup, the right panel the TGC setup.

cross section. Further below the maximum, a separation of interference and lepton-pairing effects is not possible. In both setups, the NLO EW corrections do not modify the shape of the ratio.

The left plot in figure 5 shows the distribution in the transverse mass of the reconstructed W boson, $M_T^W = M_T^{e\nu}$, as defined in eq. (3.12) in the TGC setup. The peak of the distribution is located below the W-boson mass (the reconstructed invariant W-boson mass is experimentally not accessible owing to the undetected neutrino). The quark-induced corrections follow a similar pattern as already observed in $M_T^{3\ell\nu}$: below the maximum, the subtracted virtual corrections are small (less than 1% in magnitude). Above, they constantly increase in size up to -7.5% with growing $M_T^{e\nu}$ due to logarithms of EW origin. The subtracted real corrections above 100 GeV give again an off-set of the order of -5%. Both the dip right above the maximum and the increase below that maximum represent the radiative response of the broadly peaked transverse-mass distribution: final-state radiation off the W-decay lepton shifts the numerical value of the observable closer to (further away from) the maximum. Depending on the slope of the LO prediction above (below) the maximum this decreases (increases) the relative corrections. In the inclusive setup (not shown)

JHEP10(2017)043

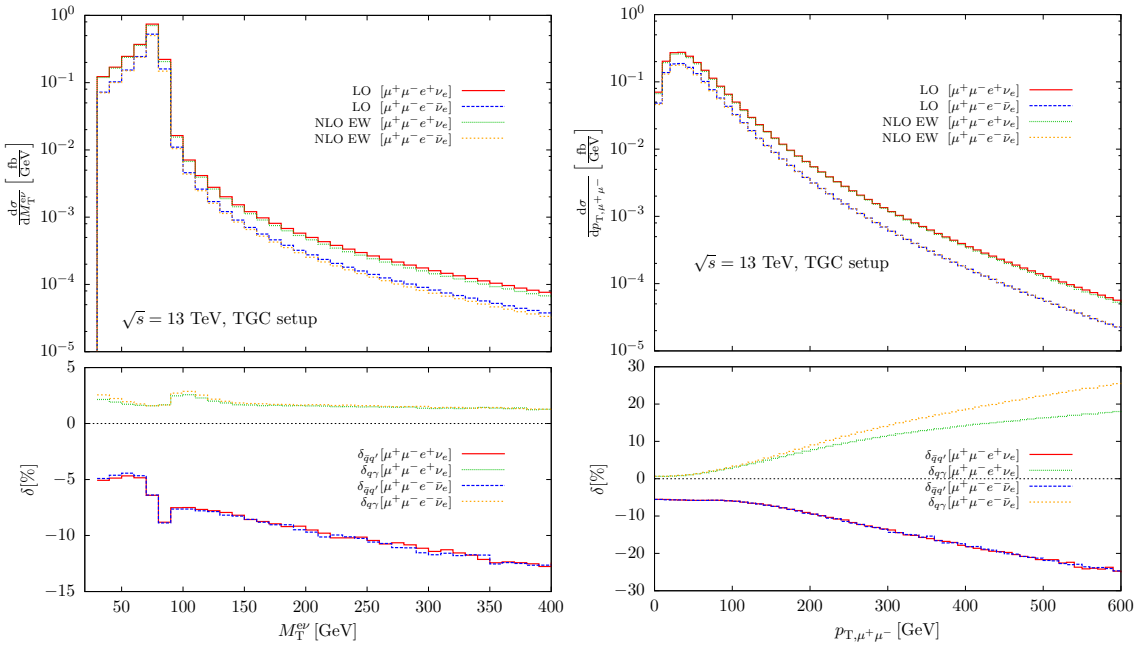

Figure 5. Distribution in the transverse mass of the reconstructed W boson (left panel) and in the transverse momentum of the $\mu^+\mu^-$ pair (right panel) in the TGC setup.

the shape of the distribution is similar to the one in the TGC setup, both for the absolute prediction and the NLO EW corrections. The relative quark-induced corrections in the inclusive setup differ from the ones in the TGC setup only by a constant shift of about +2.5%. This is expected, since the main difference between the setups, the cut around the $\mu^+\mu^-$ invariant mass in eq. (3.11), does not directly influence $M_T^{e\nu}$ as this observable does not depend on the muon momenta. The photon-induced corrections are relatively flat and do not show any particularly interesting pattern.

The right plot in figure 5 shows the transverse-momentum distribution of the $\mu^+\mu^-$ system in the TGC setup, i.e. the transverse momentum of the reconstructed Z boson. We observe the typical feature of large EW corrections in the quark-induced channels that reach −25% at 600 GeV due to EW Sudakov logarithms. We can compare this number with the corresponding results for the distribution in the Z-boson transverse momentum of the on-shell calculations of refs. [23, 24]. From the plots in these references we extract a correction of about −22% at $p_{T,Z} = 600\,\text{GeV}$. We attribute the difference of −3% to the slightly different setup and to the missing final-state radiation off muons (radiative energy loss shifts events to smaller transverse momentum and thus leads to more negative corrections). Similarly to the previously considered observables that depend on transverse momenta, the subtracted virtual corrections are small (below 1%) in the low-p_T region and start growing negative with constant slope above 100 GeV. The corrections in the low-p_T region, where the bulk of the cross section stems from, are entirely dominated by the subtracted real radiation. The fact that the corrections are flat there is again due to the invariant-mass cut (3.11). In the inclusive setup (not shown) the corrections continuously decrease in size until approaching −1.5% at zero transverse momentum. The

JHEP10(2017)043

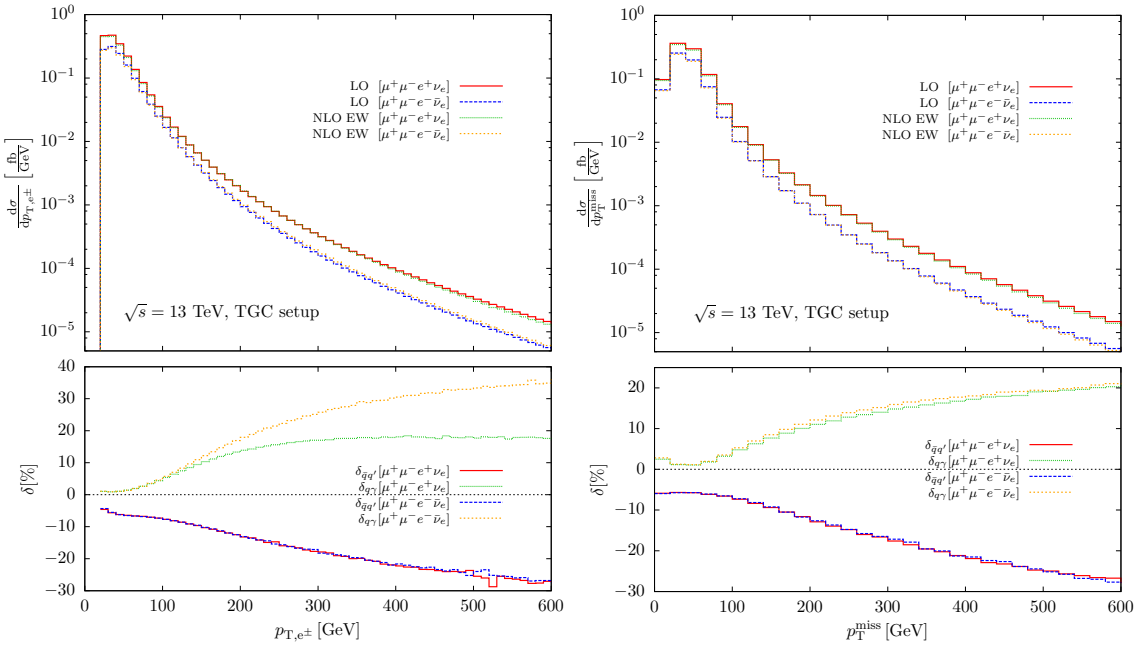

Figure 6. Distribution in the transverse-momentum of the charged W-decay lepton (left panel) and the missing-transverse momentum (right panel) in the TGC setup.

most remarkable feature of this observable is the large increase of the photon-induced contributions for high transverse momenta. At 600 GeV, they reach +18% in the ZW^+ case and even +25% in the ZW^- case, and, thus, almost compensate the large negative EW corrections from the quark-induced channels. The large difference between ZW^+ and ZW^- is caused by the different PDFs involved. In ref. [24], it has been shown that the large increase of the photon-induced cross section is mainly due to the coupling of the photon to the W boson. The photon-induced corrections presented in ref. [24] show with +28% for ZW^+ and +41% for ZW^- qualitatively a similar behaviour, though the numerical values differ. We attribute the difference mainly to the different PDF set as the ratio between the photon-induced real corrections and the purely quark-induced LO contribution is very sensitive to the employed photon PDF. The large photon-induced corrections can be reduced by imposing a jet veto [27].

The transverse-momentum distributions in figure 6 for the charged W-decay lepton (left panel) and the missing transverse momentum (right panel) show similar features as already observed in the transverse-momentum distribution of the $\mu^+\mu^-$ pair in figure 5: large negative EW corrections in the $\bar{q}q'$ channel and large positive corrections from the photon-induced contributions in the high-p_T regime that partially compensate each other. Among all transverse-momentum distributions, those for the transverse momentum of the W-decay lepton show the largest difference in the photon-induced corrections between ZW^+ and ZW^-.

The distribution in the azimuthal-angle difference of the $\mu^+\mu^-$ pair in the TGC setup is shown in the left panel of figure 7 for the ZW^+ and ZW^- mixed-flavour case. The maximum at $\Delta\phi \to \pi$ has the same origin as for the corresponding observable in ZZ production

JHEP10(2017)043

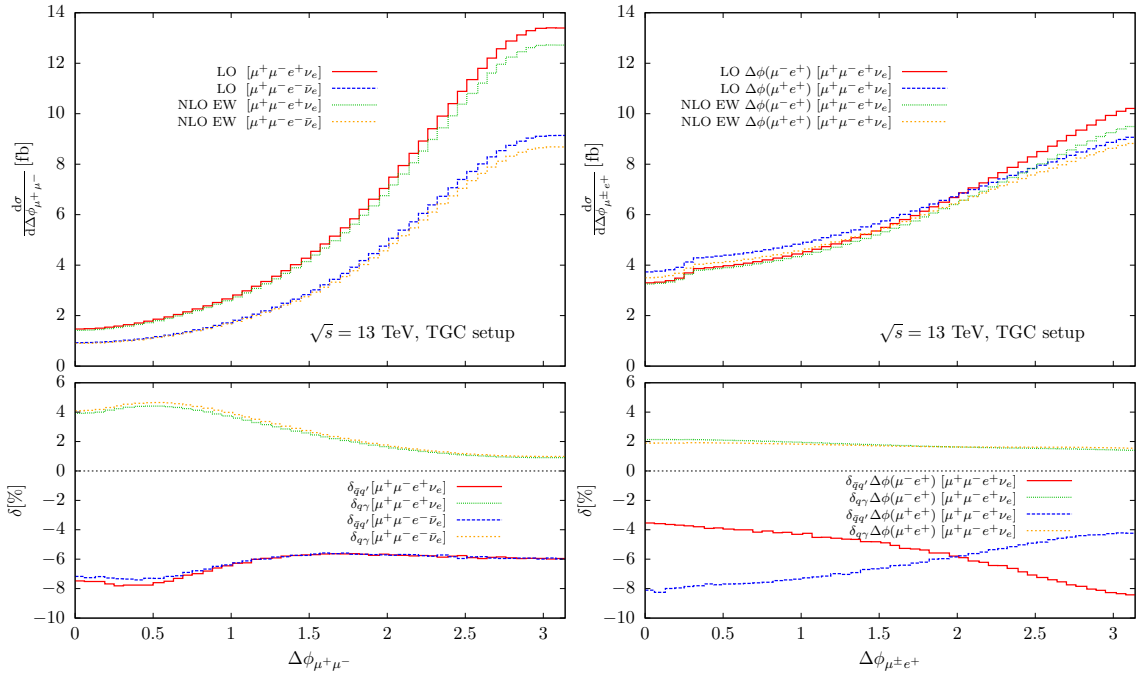

Figure 7. Distributions in the azimuthal-angle difference of the charged leptons in the TGC setup for the mixed-flavour case. The left panel shows the correlation between the $\mu^+\mu^-$ pair for ZW^+ and ZW^-. In the right panel, the correlations between the μ^-e^+ pair and the μ^+e^+ pair are plotted for the ZW^+ channel.

described in ref. [26]: the whole distribution is dominated by events in the energy region just above the pair-production threshold with two resonant vector bosons. Owing to the t-channel nature of the dominant contributions [cf. diagram (a) in figure 1], the vector bosons are preferably produced in forward direction with small momenta in the transverse plane. The Z-boson decay leptons are thus mainly back-to-back in the transverse plane which explains the maximum at $\Delta\phi \to \pi$. The EW corrections are nearly equal for both presented final states. Around the maximum, the $\bar{q}q'$ channels receive corrections of -6% as for the fiducial cross section. Towards $\Delta\phi \to 0$, the EW corrections are more enhanced and increase in magnitude up to -8%. This region is dominated by events with large transverse momenta of the Z boson and, therefore, enhanced by Sudakov logarithms. The photon-induced corrections show the opposite behaviour: there is a minimum at $\Delta\phi = \pi$ of $\sim +1\%$, and a maximum at $\Delta\phi = 0.5$ of $\sim +5\%$. Hence, both for the $\bar{q}q'$ and $q\gamma$ channels, the NLO EW corrections to $\Delta\phi_{\mu^+\mu^-}$ reflect qualitatively the behaviour of the corrections in the transverse-momentum distribution of the $\mu^+\mu^-$ pair in figure 5.

The plot on the right-hand side in figure 7 compares the azimuthal-angle difference of the μ^-e^+ pair with the one of the μ^+e^+ pair in the mixed-flavour ZW^+ final state. In both cases we observe a maximum at $\Delta\phi = \pi$, and a minimum at $\Delta\phi = 0$ resulting from boosts of back-to-back W and Z bosons. The kink at $\Delta\phi = 0.3$ is due to the lepton-separation cut in eq. (3.10). The difference between maximum and minimum is much smaller than for $\Delta\phi_{\mu^+\mu^-}$, and smallest for $\Delta\phi_{\mu^+e^+}$. The photon-induced corrections show a rather flat behaviour and are practically independent of the observable. The $\bar{q}q'$-induced

JHEP10(2017)043

corrections, however, differ significantly for the two observables: the corrections in the μ^-e^+ case decrease from -3.5% at $\Delta\phi_{\mu^-e^+} = 0$ to -8.4% at $\Delta\phi_{\mu^-e^+} = \pi$, while those in the μ^+e^+ case increase from -8.2% to -4.2% within the same range of $\Delta\phi_{\mu^+e^+}$. The observed difference is mainly caused by the real corrections and due to events close to the WZ production threshold.

Figure 8 shows various distributions in the rapidities of the charged leptons for the mixed-flavour final states of ZW^+ and ZW^- in the TGC setup. In the upper row, distributions in the rapidities of the μ^+ and the μ^- are presented. The corresponding photon-induced corrections are rather flat and almost equal for y_{μ^+} and y_{μ^-}. The quark-induced corrections show a striking difference in the curvature of the relative corrections: those for y_{μ^+} are minimal in the central region and maximal in forward direction, while it is just the other way round for y_{μ^-}. In forward direction, the difference between the corrections to the two observables amounts to 2.5% for ZW^+ and 3.0% for ZW^-. This behaviour originates from the difference in the PDFs of up and down quarks in combination with the fact that the matrix element is not symmetric under exchange of the μ^+ and μ^- momenta. The lower left plot shows the distribution in the rapidity of the $\mu^+\mu^-$ pair, i.e. the rapidity of the reconstructed Z boson. Like in the upper plots, the photon-induced corrections are flat and almost equal for ZW^+ and ZW^-. This holds also for the quark-induced corrections in the central region. In forward direction, we observe a difference between the corrections to ZW^+ and ZW^- of about one percent which can be attributed to the interplay of PDFs and subtracted virtual corrections. The lower right plot shows the distribution in the rapidity of the charged lepton from W decay. The photon-induced corrections stay at the level of 2% with sub-percent deviations between ZW^+ and ZW^-. Differences of similar size are also observed in the quark-induced corrections. Like for $y_{\mu^+\mu^-}$, we could show that the difference is induced by the PDFs and largest for the virtual corrections.

Figure 9 displays the distribution in the rapidity difference of the $\mu^\pm e^\pm$ pairs (left panel) and in the rapidity difference of the $\mu^\mp e^\pm$ pairs (right panel) for ZW^+ and ZW^- in the TGC setup. The NLO EW corrections of the quark-induced channels show characteristic percent-level differences between the ZW^+ and ZW^- case. For the same-sign pair μ^+e^+ (μ^-e^-), the corrections in the ZW^+ case (ZW^- case) have a maximum at $\Delta y = 0$ with -4% (-5%), and reach -8% (-6%) at $|\Delta y| = 5$. The maximal difference of the corrections is, thus, largest for the ZW^+ case. In the opposite-sign case ($\mu^\mp e^\pm$ pairs), the behaviour is the other way round. The corrections for ZW^+ vary between their extrema by only about 2%, while the variation for ZW^- amounts to almost 5%. The photon-induced corrections are basically equal for both final states and rather flat.

4 Conclusions

The production of a pair of a neutral and a charged vector boson with subsequent leptonic decays is a very important process for precision tests of the Standard Model of elementary particles and in searches for anomalous triple-gauge-boson couplings (TGC). In this article, the first computation of next-to-leading order (NLO) electroweak (EW) corrections to the production of three charged leptons plus missing energy at the Large Hadron Col-

JHEP10(2017)043

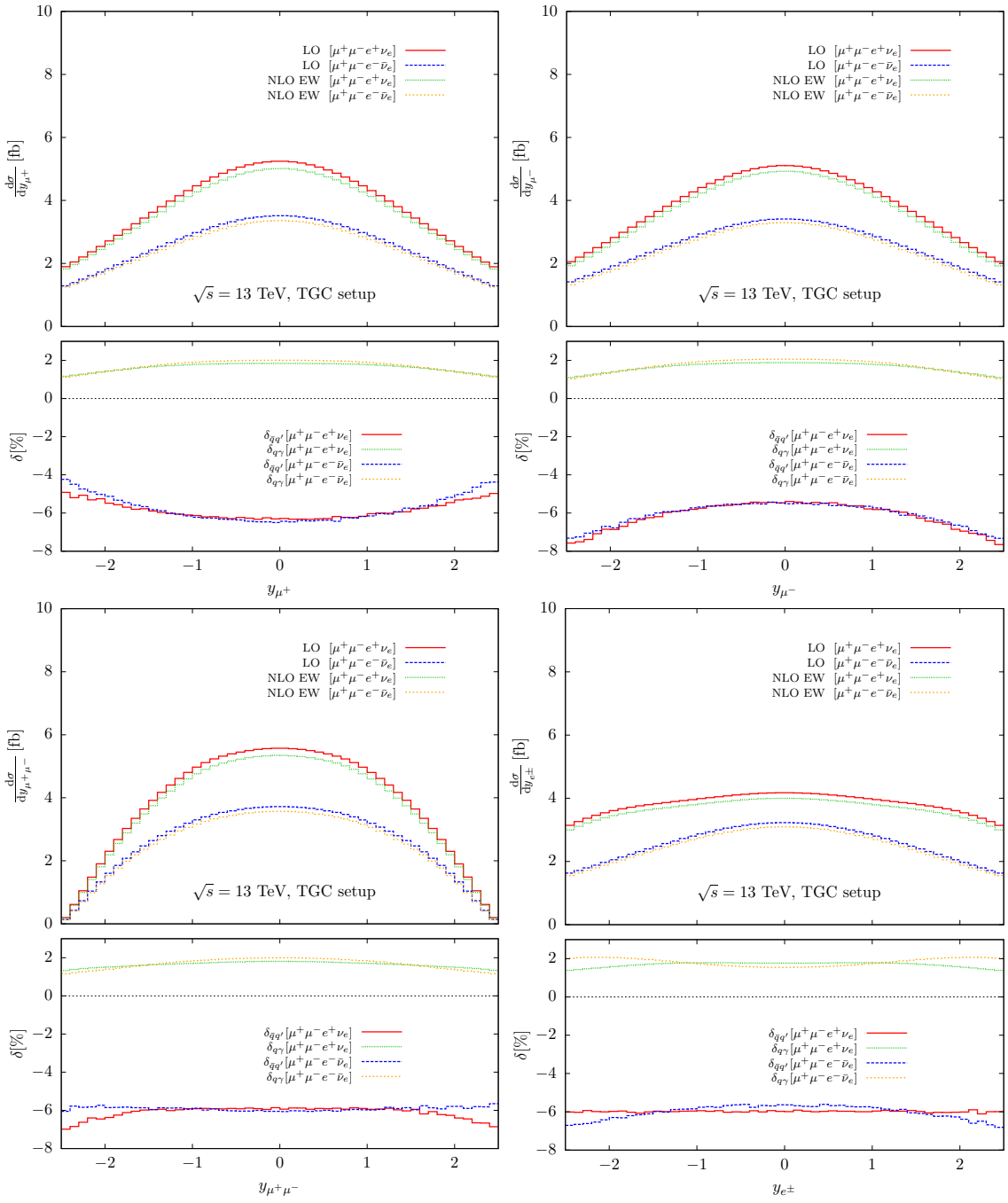

Figure 8. Distributions in the rapidities of the W and Z decay leptons in the TGC setup for ZW^+ and ZW^-: μ^+ (upper left panel), μ^- (upper right panel), $\mu^+\mu^-$ pair (lower left panel) and $e^\pm$ (lower right panel).

lider has been presented. We have analysed the four independent final states $\mu^+\mu^-e^+\nu_e$, $\mu^+\mu^-e^-\bar{\nu}_e$, $\mu^+\mu^-\mu^+\nu_\mu$, and $\mu^+\mu^-\mu^-\bar{\nu}_\mu$ applying realistic experimental phase-space cuts, first in a rather inclusive setup with minimal event selection and second in a scenario that is tailored to TGC searches. We use the complete matrix elements including all off-shell

JHEP10(2017)043

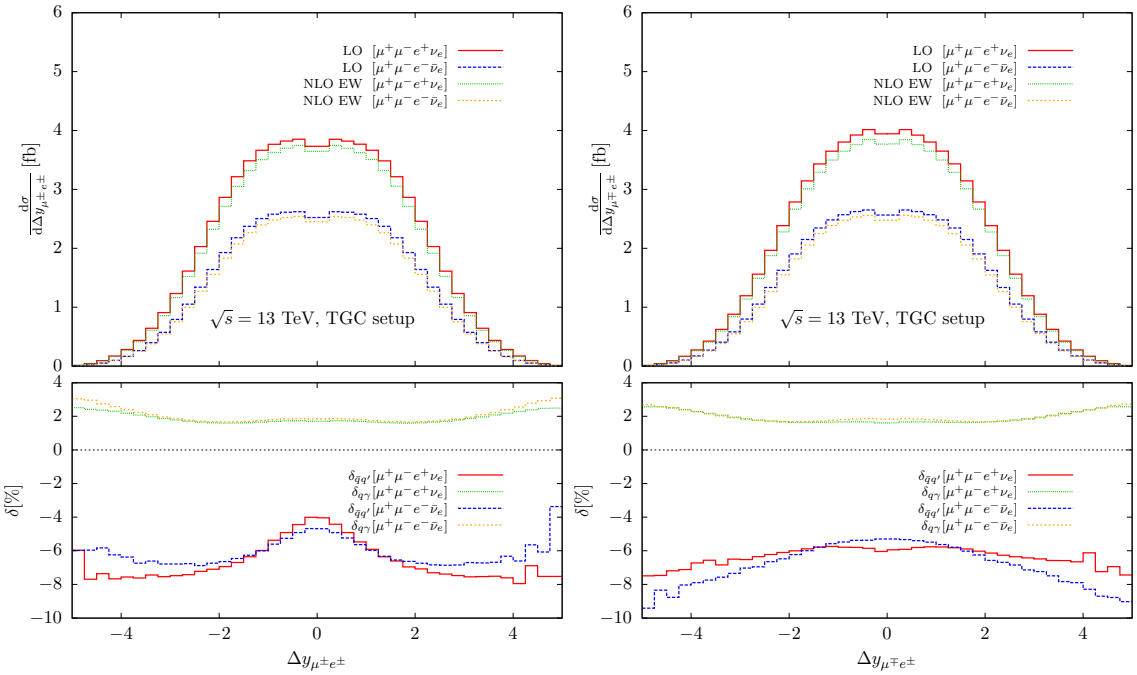

Figure 9. Distribution in the rapidity difference of the $\mu^\pm e^\pm$ pairs (left panel) and the $\mu^\mp e^\pm$ pairs (right panel) for ZW^+ and ZW^- in the TGC setup.

effects of intermediate massive vector bosons and virtual photons as well as irreducible background diagrams.

We have computed the NLO EW corrections resulting from quark-antiquark initial states as well as from initial states with photons. The photon-induced corrections raise the leading-order (LO) cross sections by about +2% in both scenarios. The quark-induced corrections depend significantly on the fiducial volume. They lower the cross section by about −3% in the inclusive case and by about −6% in the TGC setup. For the fiducial cross section, the corrections to final states with positive total charge (ZW^+) differ from those with negative total charge (ZW^-) at the sub-percent level.

At the level of differential distributions, we observe quark-induced corrections of up to −30% in the high-energy tails of distributions stemming from EW Sudakov logarithms. The photon-induced corrections show an opposite behaviour. They are positive over the whole phase space and grow with increasing transverse momenta and thus partly compensate the quark-induced corrections. Since the photon-induced contributions first occur at NLO for the considered processes, their impact can efficiently be suppressed by applying an appropriate jet veto.

Comparing the processes with opposite total charge of the final state (ZW^+ and ZW^-), we observe that the photon-induced corrections exhibit significant differences of more than 10% for certain observables. The different behaviour between the ZW^+ and ZW^- channels results from the differences in the parton distribution functions for the respective initial states. Concerning quark-induced corrections, percent-level differences between final states with opposite charge are found in rapidity distributions. Differential distributions that are

JHEP10(2017)043

sensitive to kinematic thresholds or resonances show typical radiative tails induced by photon-radiation off final-state leptons and lead to characteristic differences between the considered inclusive and TGC setups.

We have studied the impact of interference effects arising in final states with equal-flavour leptons. In the inclusive setup, they lower the fiducial cross section with respect to the mixed-flavour case at the permille level only. While this holds true also at the level of differential distributions in phase-space regions dominated by on-shell vector-boson-pair production, interference effects become sizeable and lower the cross section by up to one third in off-shell sensitive phase-space regions. If the observables or the phase-space cuts depend on the selection of equal-flavour final-state leptons (like in the considered TGC scenario), the differences between equal- and mixed-flavour processes are, in general, more pronounced and cannot exclusively be attributed to interferences. Both at LO and NLO, the shape distortions owing to lepton selection and interferences are almost equal in size.

The NLO EW corrections for WZ production presented in this article are important for precision tests of the Standard Model and its possible extensions. Taking into account that this process is meanwhile known at next-to-next-to-leading order in the strong coupling, the NLO EW corrections further reduce the theoretical uncertainty and can help to improve the exclusion limits on anomalous TGC. We advocate for a systematic inclusion of the EW corrections in future experimental analyses.

Acknowledgments

We would like to thank Stefan Dittmaier for useful discussions. The work of B.B. and A.D. was supported by the German Federal Ministry for Education and Research (BMBF) under contract no. 05H15WWCA1 and by the German Science Foundation (DFG) under reference number DE 623/6-1. The work of L.H. was supported by the Spanish MINECO grants FPA2013-46570-C2-1-P and FPA2016-76005-C2-1-P, by the grant 2014-SGR-104, and partially under the project MDM-2014-0369 of ICCUB (Unidad de Excelencia "María de Maeztu").

References

[1] ATLAS collaboration, *Measurement of WZ production in proton-proton collisions at $\sqrt{s} = 7$ TeV with the ATLAS detector*, *Eur. Phys. J.* **C 72** (2012) 2173 [arXiv:1208.1390] [INSPIRE].

[2] ATLAS collaboration, *Measurements of $W^{\pm}Z$ production cross sections in pp collisions at $\sqrt{s} = 8$ TeV with the ATLAS detector and limits on anomalous gauge boson self-couplings*, *Phys. Rev.* **D 93** (2016) 092004 [arXiv:1603.02151] [INSPIRE].

JHEP10(2017)043

[3] ATLAS collaboration, *Measurement of the $W^{\pm}Z$ boson pair-production cross section in pp collisions at $\sqrt{s} = 13$ TeV with the ATLAS Detector*, *Phys. Lett.* **B 762** (2016) 1 [arXiv:1606.04017] [INSPIRE].

[4] CMS collaboration, *Measurement of the WZ production cross section in pp collisions at $\sqrt{s} = 13$ TeV*, *Phys. Lett.* **B 766** (2017) 268 [arXiv:1607.06943] [INSPIRE].

[5] CMS collaboration, *Measurement of the WZ production cross section in pp collisions at $\sqrt{s} = 7$ and 8 TeV and search for anomalous triple gauge couplings at $\sqrt{s} = 8$ TeV*, *Eur. Phys. J.* **C 77** (2017) 236 [arXiv:1609.05721] [INSPIRE].

[6] ATLAS collaboration, *Measurement of $W^{\pm}Z$ boson pair-production in pp collisions at $\sqrt{s} = 13$ TeV with the ATLAS Detector and confidence intervals for anomalous triple gauge boson couplings*, ATLAS-CONF-2016-043 (2016).

[7] J. Ohnemus, *An order α_S calculation of hadronic $W^{\pm}Z$ production*, *Phys. Rev.* **D 44** (1991) 3477 [INSPIRE].

[8] J. Ohnemus, *Hadronic ZZ, W^-W^+ and $W^{\pm}Z$ production with QCD corrections and leptonic decays*, *Phys. Rev.* **D 50** (1994) 1931 [hep-ph/9403331] [INSPIRE].

[9] L.J. Dixon, Z. Kunszt and A. Signer, *Vector boson pair production in hadronic collisions at order α_s: Lepton correlations and anomalous couplings*, *Phys. Rev.* **D 60** (1999) 114037 [hep-ph/9907305] [INSPIRE].

[10] J.M. Campbell and R.K. Ellis, *An update on vector boson pair production at hadron colliders*, *Phys. Rev.* **D 60** (1999) 113006 [hep-ph/9905386] [INSPIRE].

[11] K. Hamilton, *A positive-weight next-to-leading order simulation of weak boson pair production*, *JHEP* **01** (2011) 009 [arXiv:1009.5391] [INSPIRE].

[12] T. Melia, P. Nason, R. Röntsch and G. Zanderighi, *W^+W^-, WZ and ZZ production in the POWHEG BOX*, *JHEP* **11** (2011) 078 [arXiv:1107.5051] [INSPIRE].

[13] P. Nason and G. Zanderighi, *W^+W^-, WZ and ZZ production in the POWHEG-BOX-V2*, *Eur. Phys. J.* **C 74** (2014) 2702 [arXiv:1311.1365] [INSPIRE].

[14] M. Grazzini, S. Kallweit, D. Rathlev and M. Wiesemann, *$W^{\pm}Z$ production at hadron colliders in NNLO QCD*, *Phys. Lett.* **B 761** (2016) 179 [arXiv:1604.08576] [INSPIRE].

[15] M. Grazzini, S. Kallweit, D. Rathlev and M. Wiesemann, *$W^{\pm}Z$ production at the LHC: fiducial cross sections and distributions in NNLO QCD*, *JHEP* **05** (2017) 139 [arXiv:1703.09065] [INSPIRE].

[16] W. Beenakker, A. Denner, S. Dittmaier, R. Mertig and T. Sack, *High-energy approximation for on-shell W pair production*, *Nucl. Phys.* **B 410** (1993) 245 [INSPIRE].

[17] M. Beccaria, G. Montagna, F. Piccinini, F.M. Renard and C. Verzegnassi, *Rising bosonic electroweak virtual effects at high-energy e^+e^- colliders*, *Phys. Rev.* **D 58** (1998) 093014 [hep-ph/9805250] [INSPIRE].

[18] P. Ciafaloni and D. Comelli, *Sudakov enhancement of electroweak corrections*, *Phys. Lett.* **B 446** (1999) 278 [hep-ph/9809321] [INSPIRE].

[19] J.H. Kühn and A.A. Penin, *Sudakov logarithms in electroweak processes*, hep-ph/9906545 [INSPIRE].

JHEP10(2017)043

[20] V.S. Fadin, L.N. Lipatov, A.D. Martin and M. Melles, *Resummation of double logarithms in electroweak high-energy processes*, *Phys. Rev.* **D 61** (2000) 094002 [hep-ph/9910338] [INSPIRE].

[21] A. Denner and S. Pozzorini, *One loop leading logarithms in electroweak radiative corrections. 1. Results*, *Eur. Phys. J.* **C 18** (2001) 461 [hep-ph/0010201] [INSPIRE].

[22] E. Accomando, A. Denner and A. Kaiser, *Logarithmic electroweak corrections to gauge-boson pair production at the LHC*, *Nucl. Phys.* **B 706** (2005) 325 [hep-ph/0409247] [INSPIRE].

[23] A. Bierweiler, T. Kasprzik and J.H. Kühn, *Vector-boson pair production at the LHC to $\mathcal{O}(\alpha^3)$ accuracy*, *JHEP* **12** (2013) 071 [arXiv:1305.5402] [INSPIRE].

[24] J. Baglio, L.D. Ninh and M.M. Weber, *Massive gauge boson pair production at the LHC: a next-to-leading order story*, *Phys. Rev.* **D 88** (2013) 113005 [arXiv:1307.4331] [INSPIRE].

[25] B. Biedermann, A. Denner, S. Dittmaier, L. Hofer and B. Jäger, *Electroweak corrections to $pp \to \mu^+\mu^- e^+ e^- + X$ at the LHC: a Higgs background study*, *Phys. Rev. Lett.* **116** (2016) 161803 [arXiv:1601.07787] [INSPIRE].

[26] B. Biedermann, A. Denner, S. Dittmaier, L. Hofer and B. Jäger, *Next-to-leading-order electroweak corrections to the production of four charged leptons at the LHC*, *JHEP* **01** (2017) 033 [arXiv:1611.05338] [INSPIRE].

[27] B. Biedermann et al., *Next-to-leading-order electroweak corrections to $pp \to W^+W^- \to 4$ leptons at the LHC*, *JHEP* **06** (2016) 065 [arXiv:1605.03419] [INSPIRE].

[28] S. Kallweit, J.M. Lindert, S. Pozzorini and M. Schönherr, *NLO QCD+EW predictions for $2\ell 2\nu$ diboson signatures at the LHC*, arXiv:1705.00598 [INSPIRE].

[29] A. Denner, S. Dittmaier, M. Roth and D. Wackeroth, *Predictions for all processes $e^+e^- \to 4$ fermions + γ*, *Nucl. Phys.* **B 560** (1999) 33 [hep-ph/9904472] [INSPIRE].

[30] A. Denner, S. Dittmaier, M. Roth and L.H. Wieders, *Electroweak corrections to charged-current $e^+e^- \to 4$ fermion processes: Technical details and further results*, *Nucl. Phys.* **B 724** (2005) 247 [*Erratum ibid.* **B 854** (2012) 504] [hep-ph/0505042] [INSPIRE].

[31] A. Denner and S. Dittmaier, *The complex-mass scheme for perturbative calculations with unstable particles*, *Nucl. Phys. Proc. Suppl.* **160** (2006) 22 [hep-ph/0605312] [INSPIRE].

[32] S. Dittmaier, *A general approach to photon radiation off fermions*, *Nucl. Phys.* **B 565** (2000) 69 [hep-ph/9904440] [INSPIRE].

[33] S. Dittmaier, A. Kabelschacht and T. Kasprzik, *Polarized QED splittings of massive fermions and dipole subtraction for non-collinear-safe observables*, *Nucl. Phys.* **B 800** (2008) 146 [arXiv:0802.1405] [INSPIRE].

[34] S. Catani and M.H. Seymour, *A general algorithm for calculating jet cross-sections in NLO QCD*, *Nucl. Phys.* **B 485** (1997) 291 [*Erratum ibid.* **B 510** (1998) 503] [hep-ph/9605323] [INSPIRE].

[35] B. Biedermann, A. Denner and M. Pellen, *Large electroweak corrections to vector-boson scattering at the Large Hadron Collider*, *Phys. Rev. Lett.* **118** (2017) 261801 [arXiv:1611.02951] [INSPIRE].

[36] B. Biedermann, A. Denner and M. Pellen, *Complete NLO corrections to W^+W^+ scattering and its irreducible background at the LHC*, arXiv:1708.00268 [INSPIRE].

JHEP10(2017)043

[37] S. Actis, A. Denner, L. Hofer, J.-N. Lang, A. Scharf and S. Uccirati, *RECOLA: REcursive Computation of One-Loop Amplitudes*, *Comput. Phys. Commun.* **214** (2017) 140 [arXiv:1605.01090] [INSPIRE].

[38] A. Denner, S. Dittmaier and L. Hofer, *Collier: a fortran-based Complex One-Loop LIbrary in Extended Regularizations*, *Comput. Phys. Commun.* **212** (2017) 220 [arXiv:1604.06792] [INSPIRE].

[39] G. 't Hooft and M.J.G. Veltman, *Scalar One Loop Integrals*, *Nucl. Phys.* **B 153** (1979) 365 [INSPIRE].

[40] W. Beenakker and A. Denner, *Infrared Divergent Scalar Box Integrals With Applications in the Electroweak Standard Model*, *Nucl. Phys.* **B 338** (1990) 349 [INSPIRE].

[41] S. Dittmaier, *Separation of soft and collinear singularities from one loop N point integrals*, *Nucl. Phys.* **B 675** (2003) 447 [hep-ph/0308246] [INSPIRE].

[42] A. Denner and S. Dittmaier, *Scalar one-loop 4-point integrals*, *Nucl. Phys.* **B 844** (2011) 199 [arXiv:1005.2076] [INSPIRE].

[43] G. Passarino and M.J.G. Veltman, *One Loop Corrections for e^+e^- Annihilation Into $\mu^+\mu^-$ in the Weinberg Model*, *Nucl. Phys.* **B 160** (1979) 151 [INSPIRE].

[44] A. Denner and S. Dittmaier, *Reduction of one loop tensor five point integrals*, *Nucl. Phys.* **B 658** (2003) 175 [hep-ph/0212259] [INSPIRE].

[45] A. Denner and S. Dittmaier, *Reduction schemes for one-loop tensor integrals*, *Nucl. Phys.* **B 734** (2006) 62 [hep-ph/0509141] [INSPIRE].

[46] E. Accomando, A. Denner and C. Meier, *Electroweak corrections to $W\gamma$ and $Z\gamma$ production at the LHC*, *Eur. Phys. J.* **C 47** (2006) 125 [hep-ph/0509234] [INSPIRE].

[47] J. Küblbeck, M. Böhm and A. Denner, *Feyn Arts: Computer Algebraic Generation of Feynman Graphs and Amplitudes*, *Comput. Phys. Commun.* **60** (1990) 165 [INSPIRE].

[48] T. Hahn, *Generating Feynman diagrams and amplitudes with FeynArts 3*, *Comput. Phys. Commun.* **140** (2001) 418 [hep-ph/0012260] [INSPIRE].

[49] T. Hahn and M. Pérez-Victoria, *Automatized one loop calculations in four-dimensions and D-dimensions*, *Comput. Phys. Commun.* **118** (1999) 153 [hep-ph/9807565] [INSPIRE].

[50] F.A. Berends, R. Pittau and R. Kleiss, *All electroweak four fermion processes in electron-positron collisions*, *Nucl. Phys.* **B 424** (1994) 308 [hep-ph/9404313] [INSPIRE].

[51] S. Dittmaier and M. Roth, *LUSIFER: A LUcid approach to six FERmion production*, *Nucl. Phys.* **B 642** (2002) 307 [hep-ph/0206070] [INSPIRE].

[52] Particle Data Group collaboration, C. Patrignani et al., *Review of Particle Physics*, *Chin. Phys.* **C 40** (2016) 100001 [INSPIRE].

[53] D. Yu. Bardin, A. Leike, T. Riemann and M. Sachwitz, *Energy-dependent width effects in e^+e^- annihilation near the Z boson pole*, *Phys. Lett.* **B 206** (1988) 539 [INSPIRE].

[54] A. Manohar, P. Nason, G.P. Salam and G. Zanderighi, *How bright is the proton? A precise determination of the photon parton distribution function*, *Phys. Rev. Lett.* **117** (2016) 242002 [arXiv:1607.04266] [INSPIRE].

[55] J. Butterworth et al., *PDF4LHC recommendations for LHC Run II*, *J. Phys.* **G 43** (2016) 023001 [arXiv:1510.03865] [INSPIRE].

JHEP10(2017)043